Atmos. Chem. Phys. Discuss., 12, 31991–32038, 2012
www.atmos-chem-phys-discuss.net/12/31991/2012/
doi:10.5194/acpd-12-31991-2012

Atmospheric Chemistry and Physics Discussions

A net decrease in the Earth's cloud plus aerosol reflectivity during the past 33 yr (1979–2011) and increased solar heating at the surface

J. R. Herman[1,2], **M. T. DeLand**[1,3], **L.-K. Huang**[1,3], **G. Labow**[1,3], **D. Larko**[1,3], **S. A. Lloyd**[1,5], **J. Mao**[1,4], **W. Qin**[1,3], **and C. Weaver**[1,4]

[1]NASA Goddard Space Flight Center, Greenbelt, MD 20771, USA
[2]Joint Center for Earth Systems Technology (JCET) Center, University of Maryland, Baltimore County, Catonsville, MD 21228, USA
[3]Science Systems and Applications (SSAI), Inc., Lanham, MD 20706, USA
[4]Earth System Science Interdisciplinary Center (ESSIC), University of Maryland, College Park, MD 20740, USA
[5]Wyle Information Services, McLean, VA 22102, USA

Received: 17 October 2012 – Accepted: 18 November 2012 – Published: 13 December 2012

Correspondence to: J. R. Herman (jay.r.herman@nasa.gov), G. Labow (gordon.j.labow@nasa.gov)

Published by Copernicus Publications on behalf of the European Geosciences Union.

Abstract

Measured upwelling radiances from Nimbus-7 SBUV, seven NOAA SBUV/2 and the AURA-OMI instruments have been used to calculate the 340 nm Lambertian Equivalent Reflectivity (LER) of the Earth from 1979 to 2011 after applying a new common calibration. The 340 nm LER is highly correlated with cloud and aerosol cover because of the low surface reflectivity of the land and oceans (typically 2 to 6 RU, where 1 RU = 0.01 = 1.0 %) relative to the much higher reflectivity of clouds plus aerosols (typically 10 to 90 RU). Because of the nearly constant seasonal and long-term 340 nm surface reflectivity, the 340 nm LER can be used to estimate changes in cloud plus aerosol amount associated with seasonal and interannual variability and decadal climate change. The annual motion of the Intertropical Convergence Zone, episodic El Nino Southern Oscillation ENSO, and latitude dependent seasonal cycles are apparent in the LER time series. LER trend estimates from 5° zonal average and from 2° × 5° latitude × longitude time series show that there has been a global net decrease in cloud plus aerosol reflectivity. The decrease in global $\cos^2$ (latitude) weighted average LER from 60° S to 60° N is 0.79 ± 0.03 RU over 33 yr, corresponding to a 3.6 ± 0.2 % change in LER. Based on energy balance partitioning (Trenberth et al., 2009) this corresponds to an increase of 2.7 W m^{-2} of solar energy reaching the Earth's surface (an increase of 1.4 % or 2.3 W m^{-2}) absorbed by the surface, which is partially offset by an increase in longwave cooling to space. Most of the decreases in cloud reflectivity occur over land, with the largest decreases occurring over the US (−0.97 RU decade^{-1}), Brazil (−0.9 RU decade^{-1}), and Central Europe (−1.35 RU decade^{-1}). There are reflectivity increases near the west coast of Peru and Chile (0.8 ± 0.1 RU decade^{-1}) over parts of India, China, and Indochina, and almost no change over Australia. The largest Pacific Ocean change is −2 ± 0.1 RU decade^{-1} over the central equatorial region associated with ENSO. An area in Central Greenland shows a decrease in reflectivity of −0.3 ± 0.03 RU decade^{-1} caused by cloud and possible surface changes.

ACPD

12, 31991–32038, 2012

A net decrease in the Earth's cloud plus aerosol reflectivity 1979–2011

J. R. Herman et al.

1 Introduction

The Earth's energy balance is mostly determined by the shortwave solar energy received at the Earth's surface, shortwave energy reflected back to space, and longwave energy emitted to space. Both the incoming solar radiation, which includes near ultraviolet (NUV), visible, and near infrared (NIR) wavelengths, and the emitted outgoing longwave infrared radiation (IR), are affected by the presence of clouds and aerosols. Clouds can simultaneously reflect shortwave radiation back to space before it reaches the Earth's surface (resulting in cooling) and act as a thermal blanket to trap longwave radiation (heating) in the lower atmosphere. One of the key questions concerning global warming is the response of clouds as surface temperatures change. Many model studies showing temperature increases indicate a positive feedback for clouds reflecting energy back to space (IPCC, 2007). That is, as the average temperature increases cloud cover decreases so that more solar energy reaches and is absorbed by the Earth's surface, which is partially offset by increased outgoing IR radiation. It is generally agreed that there has been a statistically significant increase in global average temperature since 1979. An estimate of the increase is 0.15 °C decade^{-1} (Hansen et al., 2010) or about 0.5 °C since 1979. However, in response to the temperature increase, the direction of cloud feedback based on observations is still an open question.

The global heat flow can be partitioned approximately as 341 W m^{-2} average incoming solar radiation, 102 W m^{-2} reflected back to space, and 239 W m^{-2} from outgoing long-wave radiation (Kiehl and Trenberth, 1997; Trenberth et al., 2009; Stevens and Schwartz, 2012). Of the 102 W m^{-2} reflected radiation, 74 W m^{-2} is reflected by clouds and aerosols, 5 W m^{-2} by the molecular atmosphere, and 23 W m^{-2} by the surface. Clouds also block some of the longwave radiation that would be emitted back to space, so that a decrease in global cloud amount would increase the amount of solar radiation reaching the Earth's surface (more heating), but also increase the amount radiated back to space (more cooling). Depending on the effect of clouds on longwave radiative forcing, a global decrease in cloud plus aerosol reflectivity could cause an increase

ACPD
12, 31991–32038, 2012

A net decrease in the Earth's cloud plus aerosol reflectivity 1979–2011

J. R. Herman et al.

in net heating. This paper discusses one aspect contributing to the energy balance, namely the change in the Lambert Equivalent Reflectivity (LER) of the Earth's cloud plus aerosol amounts as seen from space for the past 33 yr (1979 to 2011).

Since the long-term wavelength-integrated top-of-the-atmosphere (TOA) solar irradiance is believed to be relatively stable (to within 0.1 %) over recent history (Kopp and Lean, 2011), small changes in the earth's albedo can have a significant impact on the net radiation budget affecting climate change. Previous estimates of cloud cover change have been made using the International Satellite Cloud Climatology Project (ISCCP) data archive (Schiffer and Rossow, 1983) derived from visible and infrared (IR) measurements obtained from a variety of different satellites (polar orbiting and geostationary). The problems of joining the disparate ISCCP data sets, starting in 1979, to produce an accurately calibrated long-term time series needed to estimate changes in short-wave energy reflected back to space has been reviewed by Norris and Slingo (2009). One of the more accurate cloud data sets is from the CERES instrument starting on TRMM in a low inclination tropical orbit and continuing on the polar orbiting TERRA satellite starting in 1999 and AQUA in 2002. Two other long-term cloud data sets exist, AVHRR and HIRS, which have diurnal cloud variation from drifting orbits. An analysis of ISCCP cloud frequency (Wylie et al., 2005) shows a strong decrease over land for latitudes 20° N to 60° N that was not seen in corresponding HIRS observations. ISCCP shows a larger decrease over 20–60° N oceans while HIRS shows a small increase. An analysis (Evan et al., 2007) suggests that the long-term decreases in cloud cover reported from the ISCCP data may not be reliable, but are instead related to uncorrected satellite viewing geometry effects.

2 Solar Backscatter UltraViolet (SBUV) data

In October 1978, the first of a series of well calibrated UV measuring satellite instruments, SBUV (Solar Backscattered Ultra Violet) instrument was launched onboard the Nimbus-7 spacecraft for the purpose of measuring changes in the Earth's ozone amount. The measurements were continued with overlapping data by a series of NOAA SBUV/2 instruments (1985 to present). A summary of these instruments is given in Table 1. The longest wavelength channel, 340 nm Δ1.1 *nm* FWHM (Full Width Half-Maximum), was chosen in order to measure radiances with almost no ozone absorption. Backscattered 340 nm radiances provide a useful measure of cloud plus aerosol reflectivity amount, since it is only minimally affected by changes in the surface (vegetation and ocean color).

SBUV instruments measure nadir-view earth radiances with a double monochromator scanning sequentially through 12 wavelengths between 252–340 nm. Each wavelength sample requires 2 s, and a full scan sequence is completed in 32 s while the spacecraft moves at 7 km s^{-1}. The radiances used for deriving LER are obtained from the 339.8 Δ1.1 *nm* (Δ = full-width at half-maximum, FWHM) band for the Nimbus-7 SBUV and seven NOAA SBUV(/2) instruments. Both the backscattered radiance I_{refl} and solar irradiance I_{solar} are measured at twelve discrete narrow-bandwidth ultraviolet wavelengths: nominally 256, 273, 283, 288, 292, 298, 302, 306, 312, 318, 331 and 340 nm. The exact operational wavelength used for this study varies between 339.75 nm and 339.92 nm for the different instruments, with a bandpass of 1.1 nm FWHM. The SBUV/2 instrument field of view is 11.13° × 11.13°, which produces a nadir footprint of 168 km × 168 km (equivalent to 1.5° latitude × 1.5° longitude at the Equator). The earlier Nimbus-7 SBUV (1978–1990) footprint is slightly larger because the satellite flew in a higher orbit. All of the data products are produced from normalized radiances $I_{\text{refl}}/I_{\text{solar}}$ to minimize the effects of instrument calibration changes.

The SBUV-SBUV/2 data give nearly complete global coverage (80° N to 80° S) every 7 to 10 days for the entire 33-yr period, consisting of 19.2 million individual observations taken by the seven instruments, or a mean of 68 independent LER observations per 5° latitude band per day with some overlap between instruments. After applying common calibration, overlapping data are averaged together to form a single time series of 340 nm LER. Five of the instruments (NOAA-16, -17, -18, -19 SBUV/2, and OMI) continue to take daily observations into 2012, of which the first 3 are used to estimate long-term change in LER. For those SBUV/2 instruments that had drifting orbits (slowly changing equator crossing times), diurnal changes in LER were removed (Labow et al., 2011) by correcting to noon values.

The TOMS (Total Ozone Mapping Spectrometer) instruments (Nimbus-7/TOMS NT and Earth Probe TOMS EP) are not included in the combined 33-yr LER data set because of remaining problems with the photomultiplier detector hysteresis effects (NT) and scan mirror degradation (EP). The hysteresis effect concerns the emergence of a photomultiplier tube instrument from night into bright daylight scenes, where the photomultiplier tube's anode has not had time to thermally equilibrate. Hysteresis effects for the SBUV series are not as severe, and have been corrected.

The Ozone Monitoring Instrument (OMI) onboard the AURA spacecraft is a hyperspectral CCD instrument that also is used to measure 340 nm LER. This study does not include the OMI 340 nm LER in the LER trend analysis in order to keep the type of observation consistent for the entire 33 yr. An analysis including OMI data shows that it does not change the trend results significantly.

The 340 nm derived reflectivity data set provides an alternate estimation for the effect of cloud plus aerosol cover to that provided by the ISCCP, HIRS, and AVHRR data records. There are key differences in the data sets: (1) The 340 nm LER is not significantly affected by the ground reflectivity ($R_G < 0.06$) compared to visible or near IR wavelengths. (2) The satellites are all of the same type (nadir viewing polar orbiting SBUV and SBUV/2), which are all able to see the Arctic, Antarctica, and Greenland for in-flight calibration or calibration validation. (3) Some of the SBUV/2 instruments were compared with the accurately calibrated Space Shuttle SBUV (SSBUV) flown 8 times between 1989 and 1996. (4) The quantity measured, Lambert Equivalent Reflectivity LER, is a direct measure of energy reflected from clouds and aerosols. (5) The LER data are corrected for diurnal variation in cloud cover in a manner that does not remove long-term changes. (6) Unlike ISCCP, the SBUV LER data are not able to separate the different types of clouds, do not separately give optical depth and cloud fraction, and cannot separate clouds from aerosols.

The previous shorter period LER trend estimates (Herman et al., 2009, 2010) were based on measured radiances at 380 Δ0.5 *nm* from Nimbus-7/TOMS (N7T) and at 412 Δ10 *nm* from SeaWiFs (SW). Prior to recalibrating the SBUV and SBUV/2 instruments, it was shown that most of the major reflectivity features were commonly observed at times when there was overlap between the instruments (Herman et al., 2009, Fig. 8). However, the relative calibration between the various satellite instruments was inadequate for the estimation of long-term trends over the entire data record. For the overlap period 2001 to 2006, NOAA-16 SBUV/2 was shown to agree closely with the zonal average trend estimates from SeaWiFs (1997 to 2008). Finally, latitude × longitude trend estimates were made for N7T and SeaWiFs (Herman et al., 2009, Fig. 13), which showed significant LER decreases over land areas in the Northern Hemisphere as well as some localized increases in the equatorial Pacific Ocean and near the west coast of South America. However, there are also significant LER differences between the two observing periods based on N7T (380 Δ0.5 *nm*) and SeaWiFs (412 Δ10 *nm*), which may partly depend on instrumental characteristics. Since the SBUV and SBUV/2 are the only series of instruments having very similar observing characteristics, span the entire data record 1979 to present, and have a new common calibration, the LER time series (60° S–60° N) are constructed entirely from their recalibrated measured radiances.

3 Satellite instrument calibration

The primary measured quantity used in all derived products is the ratio of nadir-viewed backscattered earth radiances to measured solar irradiance at each wavelength. Solar irradiance is measured by deploying a diffuser to reflect sunlight into the entrance slit of the monochromator as the satellite crosses the terminator into the night side. The solar diffuser is the only element not common to the optical path in the two measurements. As a result, many factors in the instrument sensitivity calibration are canceled in the ratio of measured earth radiances to measured solar irradiance (directional albedo) used

ACPD
12, 31991–32038, 2012

A net decrease in the Earth's cloud plus aerosol reflectivity 1979–2011

J. R. Herman et al.

for the LER retrieval. Characterizing changes in diffuser reflectivity is a key element in determining time-dependent calibration changes.

Each SBUV instrument was calibrated in the laboratory prior to launch. The pre-launch calibration procedures include measuring and characterizing the monochromator wavelength scale and band pass, electronic offset, photomultiplier tube (PMT) output inter-range gain ratios, thermal response, nonlinearity, radiance and irradiance sensitivity, solar diffuser reflectivity, and diffuser reflectivity angular dependence (Frederick et al., 1986). The radiance and irradiance calibrations are traceable to standard NIST (National Institute of Standards and Technology) quartz-halogen tungsten-coated filament (FEL) lamps and diffuser BRDF (Bi-Directional Reflectance Distribution Function) standards (e.g., Huang et al., 1998; Georgiev and Butler, 2007). These measurements are performed using the same laboratory configuration (Fegley and Fowler, 1991). The only difference between the radiance and irradiance calibration is the use of a laboratory diffuser deployed in the same position as the solar diffuser used for in-flight solar irradiance measurements. Therefore, the albedo calibration (ratio of radiance sensitivity to irradiance sensitivity) depends only on the diffuser BRDF characterization rather than the lamp irradiance standard.

On-orbit validation of the albedo calibration for the earlier SBUV/2 instruments is based, in part, on coincidence analysis with Shuttle SBUV (SSBUV) data from eight flights between 1989 and 1996. Each SSBUV flight had both prelaunch and post-launch laboratory calibrations traceable to laboratory BRDF standards. The laboratory standards for the SSBUV-6, SSBUV-7, and SSBUV-8 flights were also used for all SBUV/2 instruments from NOAA-14 onward, and are designed to be more accurate than previous standards (Janz et al., 1995). In the present LER study, NOAA-11 albedo calibration is revised to be consistent with SSBUV-6. And, the N7-SBUV and NOAA-9 albedo calibrations are adjusted to the current laboratory standard, based on the coincidence radiance comparison with NOAA-11.

The prelaunch albedo calibration can also be validated on-orbit using measurements of Antarctic plateau regions, as described by Jaross and Warner (2008). NOAA-17

ACPD
12, 31991–32038, 2012

and NOAA-19 LER values over Antarctica are in good agreement with NOAA-11 and NOAA-14 measurements (after adjustments based on SSBUV coincidences in March 1994 and January 1996). NOAA-16 and NOAA-18 LER values were found to be approximately 6 % lower than concurrent NOAA-17 data, so their calibrations were adjusted upwards. Further details are given in DeLand et al. (2012).

Nimbus-7 SBUV and Nimbus-7 TOMS radiance measurements were originally observed to be as much as 10 % low when emerging from darkness in the Southern Hemisphere (SH). This behavior, termed "hysteresis", was caused by a delay in the PMT anode reaching thermal equilibrium from exposure to the backscattered radiances. A correction was developed for Nimbus-7 SBUV by comparing PMT signals with concurrent data from a reference diode that does not have this problem. DeLand et al. (2012) provides additional details about the correction procedure, which has an uncertainty of approximately 0.5 %. The impact on LER data is mainly at polar latitudes in the SH (Southern Hemisphere) summer, but can extend to the Equator during SH winter. Since NOAA-9 measured the 340 nm radiance with PMT cathode output at solar zenith angles SZA less than 80°, its 340 nm LER data is not affected by hysteresis, but has other uncharacterized anomalies that reduce its accuracy. The procedures to correct NOAA-9 anomalies and the Nimbus-7 SBUV hysteresis problem over Antarctica are given in detail by Wellemeyer et al. (1996) and DeLand et al. (2001).

The SBUV/2 instruments use emission lines from an on-board mercury lamp to monitor diffuser reflectivity changes in orbit (Weiss et al., 1991), as well as changes from prelaunch laboratory values to those in-orbit. Errors in the goniometric calibration of the diffuser can also be evaluated and corrected using the solar irradiance measurements (Ahmad et al., 1994). All instruments from NOAA-11 onward have used this system to monitor the time-dependent change of the albedo calibration in orbit. For Nimbus-7 SBUV and NOAA-9 SBUV/2, an alternate procedure involving more frequent solar exposures was developed to characterize diffuser changes (Schlesinger and Cebula, 1992), which was less reliable than the on-board calibration system.

ACPD
12, 31991–32038, 2012

The analysis of 340 nm radiance measurements over Antarctic snow/ice covered regions provides additional validation for the albedo calibration time dependence, as described by Huang et al. (2003) and DeLand et al. (2012). For NOAA-14 and NOAA-16, the snow/ice radiance results agree with the onboard calibration system within their combined long-term uncertainty (~ 1 %). For NOAA-11, NOAA-17, and NOAA-18, the snow/ice radiance results are used for the time dependence calibration of the 340 nm channel, which is also validated in the ozone product analysis (DeLand et al., 2012).

The Standard calibration procedures were developed for estimating ozone amounts based mostly on ratios of UV wavelengths (306, 312, 318, and 331 nm). While the calibration procedures were also applied to 340 nm radiances, a comparison of the overlapping 340 nm LER time series from different SBUV SBUV/2 instruments over the Antarctic plateau showed that there were still differences. To remove these differences, we assume that there has been no long-term change in the reflectivity of the Antarctic plateau over the 33-yr period of our data set to establish the final calibration for each instrument represented in the LER product. The average LER for each instrument was calculated during each SH summer season (December–January) mostly in the solar zenith angle range SZA = 60°–70°. When satellite orbit drift makes this SZA range unavailable in some years, we calculate the seasonal average LER values using SZA = 70°–78° and scale this value to 60°–70° conditions using a linear fit for SZA 60° to 80° measured during the satellite's first year in orbit. Four of the SBUV instruments used have absolute calibrations that are directly traceable to NIST standards, either through prelaunch calibration (NOAA-17 and NOAA-19) or through SSBUV coincidence analysis (NOAA-11, NOAA-14). The average of all summer LER values was calculated from these four instruments to define a reference Antarctic LER value of R_{avg} = 96.92 RU with a standard deviation of 0.51 RU (where 1 RU = 0.01 = 1.0 %). NOAA-11 data from 1992 were excluded from this calculation to remove the effects of the Mt. Pinatubo volcanic eruption. Small adjustments (typically less than ±0.5 %) were then made to each instrument's calibration so that its average Antarctic LER value also equaled R_{avg}. A linear fit to all adjusted Antarctic LER values (excluding 1992 data) gives a long-term trend of 0.00 ± 0.20 RU over 33 yr, as shown in Fig. 1. This result shows that the calibration uncertainty is sufficiently small to permit determining decadal trends larger than $0.2/3.3 = 0.06$ RU at other latitudes.

4 Lambertian Equivalent Reflectivity (LER)

Lambertian Equivalent Reflectivity R is calculated by requiring that the measured depolarized normalized radiance I_{SM} matches the calculated normalized radiance I_{S} at the observing position of the satellite (Eq. 1) by adjusting a single free parameter R in the formal solution of the radiative transfer equation (Chandrashekar, 1956; Herman et al., 2001).

$$I_{\mathrm{S}}(\Omega,\theta,R,P_0) = \frac{R I_{\mathrm{d}}(\Omega,\theta,P_0) f(\Omega,\theta,P_0)}{1 - R S_{\mathrm{b}}(\Omega,P_0)} + I_{\mathrm{d0}}(\Omega,\theta,P_0) = I_{\mathrm{SM}} \tag{1}$$

where
Ω = ozone amount
θ = viewing geometry (solar zenith angle, satellite look angle, azimuth angle)
R = LER at P_0 ($0 < R < 1$)
P_0 = pressure of a surface with reflectivity R at the local ground altitude.
S_{b} = fraction scattered back to P_0 from the atmosphere
I_{d} = sum of direct and diffuse irradiance reaching P_0
f = fraction of radiation reflected from P_0 reaching the satellite
I_{d0} = radiance scattered back from the atmosphere for $R = 0$ and $P = P_0$.

The units of reflectivity are frequently given in percent that is defined as 0 % for a completely absorbing dark surface and 100 % for a totally reflecting surface. To avoid confusion between absolute reflectivity with relative percent changes in reflectivity, the LER is expressed in "Reflectivity Units" or RU rather than percent ($0 < \mathrm{LER} < 100$ RU).

Satellites with comparatively large FOVs, such as the $180 \times 180\,\mathrm{km}^2$ FOV for SBUV and $168 \times 168\,\mathrm{km}^2$ for SBUV/2, containing a mixture of sub-pixel views of the surface and clouds, tend to appear Lambertian because of the blurring and averaging of geometric features. Satellites with small FOVs (e.g., $1 \times 1\,\text{km}^2$ from MODIS) are likely to resolve major cloud and surface irregularities, instead of averaging over them, so that the resolved features may not exhibit Lambertian behavior.

All of the radiative transfer calculations are performed using plane parallel geometry with spherical geometry corrections applied for all solar zenith angles. To avoid errors in the correction, the data are limited to SZA $\leq 80^{\circ}$. For the SBUV and SBUV/2 series, the viewing angle is always 0° (nadir viewing). Shadows of elevated cloud decks upon the lower clouds may lower the apparent LER for a given cloud amount as a function of latitude and season. Other situations, such as thin multi-layer cloud decks can increase the LER because of inter-layer reflections. Because of this, the LER is not a measure of cloud + aerosol amount, but rather an estimate of the amount of energy reflected back to space or transmitted T to the earth's surface (approximately $T = (100-R)/(100-R_G)$) (Herman et al., 2009), where R_G is the 340 nm LER of the Earth's surface.

Previous studies have used BUV-type instruments to compile climatologies and time series of LER or estimated minimum Surface LER (SLER) (Herman and Celarier, 1997; Herman et al., 2001, 2009; Kleipool et al., 2008) as a function of location and month. In the absence of snow or ice, the UV surface LER is typically well below 10 RU. These studies have shown that the LER over land is generally 2–4 RU in the NUV (340–380 nm), and up to 10 RU in small desert regions such as in Libya. There is little seasonal variation in NUV land reflectivity compared to the visible and near IR wavelengths except in the presence of snow/ice. LER over ocean varies from 4–6 RU, with small regions of up to 9 RU. Lower ocean LERs correlate with regions of phytoplankton growth, as chlorophyll *a* and other aquatic chromophores that absorb in the NUV. Higher ocean reflectivities correlate with comparatively clear ocean water. An estimate of the global average surface LER for scenes without snow or ice is about 5 RU based on Herman and Celarier (1997).

Histograms for LER frequency of occurrence for typical scenes are given in Herman et al. (1997) and Kleipool et al. (2008), with the lowest occurrences corresponding to

ACPD
12, 31991–32038, 2012

nearly aerosol- and cloud-free scenes. While it is difficult to obtain completely cloud-free scenes with a large satellite footprint (relative to the size of individual clouds or mesoscale cloud formations), the minimum values of LER are taken as a slight over-estimate of surface reflectivity as observed from space over many years of daily data. Instruments with a higher spatial resolution (smaller FOV), such as OMI or MODIS, are statistically more likely to provide cloud-free scenes through the gaps between cloud formations than SBUV.

The 340 nm nadir-viewing observations in this study assure that the satellite look or viewing angle is uniform and free of specular reflection (Sun glint). A depolarizer on the instruments removed sensitivity to Rayleigh scattering polarization effects (Heath et al., 1975). Data in this analysis is restricted to 60° N–60° S so as to remove most of the effect of persistent snow/ice cover, although snow and ice are still a factor in the high northern latitude boreal winter months. There is almost no land at high southern latitudes, 45° S–60° S, upon which snow can accumulate. The effect of surface winds affecting ocean wave brightness (white-caps) is included in the calculated LER.

LER represents the combined cloud, aerosol (including haze) and surface scene reflectivity as observed from space. Changes in LER are mostly caused by clouds and aerosols, except in regions covered by snow/ice (e.g., Greenland). An example from a single day, 10 September 2008, is shown in Fig. 2 using the daily imaging capabilities of OMI. The main patterns are higher reflectivities towards the polar regions, an equatorial band of clouds at about 5° N, and local minima (more cloud-free) at about 20° N and 20° S. Some of the smaller features are frequently recurring, such as the cloud plumes going south-eastward from Argentina, Southern Africa, and Australia. Significant sulfate aerosols, which typically rise to an altitude of 3–5 km when well away from their sources, can sometimes increase the nadir-viewing LER of a scene up to 15 RU relative to a clear-sky background. Soot, smoke, desert dust, volcanic-ash, black carbon and organic aerosols absorb in the NUV and can decrease the scene reflectivity.

While there is substantial daily variability in both cloud amount (fraction of area covered) and patterns, the general seasonal reflectivity features repeat each year with

ACPD
12, 31991–32038, 2012

small shifts in location. In addition, there are some quasi-cyclic features related to atmospheric oscillations (e.g. the 2.3 yr Quasi-Biennial Oscillation, QBO, and the more irregular El Nino and La Nina Southern Oscillations). These oscillations have well-known effects on weather, so that long-term secular changes are of interest in climate studies.

The combined 33-yr 340 nm SBUV LER data record has been used to show that reflectivity related to the amount of cloud cover varies systematically as a function of time throughout the day, with a minimum near noon over the oceans and a maximum during the afternoon over land (Labow et al., 2011). The corresponding effects of LER diurnal variability that arise from different SBUV/2 instruments operating at different local times have been partially removed by correcting the data to noon-time values. Maximum correction of LER values to their noon-normalized equivalents is typically less than 2 RU.

5 Zonal average LER

The 340-nm radiance data used to form the zonally averaged LER time series in 5° bands were derived from newly re-calibrated production files for the SBUV instruments. Aside from the new Antarctic ice radiance common calibration, no smoothing or adjustments have been made to make the LER values agree at overlapping times at other latitudes. When the satellite data sets overlap, the LER values are averaged using equal weights. The combined zonally averaged time series are shown in Fig. 3 for every other 5° latitude band for both hemispheres and all the latitude bands in Fig. 4. There are some missing data at high southern latitudes caused by the drifting orbits of the earlier SBUV/2 satellites. The presence of drifting orbits in the SBUV/2 LER time series requires a correction for LER measured at different times of the day to local noon values (Labow et al., 2011), since there is significant systematic variability in cloud amount during the day over both land and oceans as a function of latitude.

ACPD
12, 31991–32038, 2012

In the equatorial region represented by 17.5° N to 17.5° S, the annual maxima occur in June in the Northern Hemisphere (NH) and in January in the Southern Hemisphere (SH). This corresponds to the clouds following the annual motions of the inter-tropical convergence zone (ITCZ). Once outside of the ITCZ at 27.5° , the annual cycle weakens, especially in the SH. In the NH there is a relatively small peak caused by winter cloud conditions occurring over the land. The corresponding zonal band in the SH is mostly water. From 30° N to 60° N, the annual cycle is dominated by land conditions with heavy cloud cover plus snow in the winter causing a maximum LER in January. The corresponding 30–60° zone in the SH is more complicated. There is a weak winter signal from 35° S to 40° S with an LER maxima occurring in June. In the 45° S to 50° S the annual cycle is dominated by the ocean cloud cover with little coherent annual cycle. Finally, at higher latitudes 55° S to 60° S the annual cycle reappears, but with the maxima occurring in the spring (October–November) with maximal cloud amount after winter cooling (Haynes et al., 2011). This region corresponds to the southern polar vortex wind system, associated with the Antarctic ozone hole, which maximizes in areal extent in September–October and breaks up in October to November.

Figure 4 shows an alternate representation of the multi-year zonal average LER variability and annual cycles based on monthly averaged data. The figure shows the lack of symmetry between the NH and SH with a local June maximum at 7.5° N (green) and the minimum LER at about 17.5° in each hemisphere. The phasing of the annual maxima and minima shifts as a function of latitude. The highest LER are in the near-polar regions, with the annual average LER in the Southern Hemisphere higher than that in the Northern Hemisphere.

Figure 5a shows the 33-yr annual average noon-normalized reflectivity as a function of latitude, with the equatorial region having a pronounced hemispherical asymmetry (a maximum at 7.5° N and two minima at 17.5° N and 22.5° S). The noon normalization limits the latitude range to ±60° in Fig. 5a, whereas the OMI LER (Fig. 5b) is in a near-noon orbit (1330) and can be extended to ±85°. The 7.5° N offset maxima corresponds to the Inter-Tropical Convergence Zone (ITCZ) which has annual mean position

ACPD
12, 31991–32038, 2012

between 5° N and 10° N, but shifts northward during boreal summer and southward during boreal winter. The two minima at 17.5° N and 22.5° S correspond to the subsidence side of Hadley circulation dominated by the subtropical high-pressure belts. The reflectivity difference in the two minima are related to the ratio of land to water in the two hemispheres, with oceans having more persistent low, non-precipitating cloud cover than land, mainly in the west side of continents underlying cold ocean currents. The latitudinal dependence of the LER curve in Fig. 5a is similar to the CERES reflected shortwave flux (Stevens and Schwartz, 2012, their Fig. 9). Figure 5b shows the seasonal variation of the zonal average reflectivity as derived from 4 yr of OMI 340 Δ1.1 *nm* LER data. During the NH summer and autumn months (May to October) the local equatorial LER maximum is located at about 8° N and shifts to about 4° N during the winter and spring months (November to April). In the NH, the winter (December to February) LER is higher than in the summer (June to August) from 25° N to 80° N with a larger difference than in the SH winter (June to August) compared to the SH summer (December to February). The hemispheric differences in the seasonal behavior of the LER are caused by the much smaller land to ocean ratio in the SH.

There is a strong correlation of the equatorial LER (5° S–5° N) with the Multivariate El Nino Southern Oscillation Index (MEI) (Wolter and Timlin, 1993, 1998), which can be found at: http://www.esrl.noaa.gov/psd/enso/mei/table.html. MEI is composed from a principal component analysis of a combination of six variables: (1) sea-level pressure, (2) zonal and (3) meridional components of the surface wind, (4) sea surface temperature, (5) surface air temperature, and (6) total cloudiness fraction of the sky. Figure 6 shows a comparison between the equatorial cloud cover in two zonally averaged LER time series for the bands 0° to 5° N and 0° to 5° S. The daily LER data are time filtered by using a 90-day low-pass filter to correspond with the MEI data. In Fig. 6 the MEI data (approximately in the range MEI = ±3) are scaled by adding the constant 33-yr average LER to the MEI (MEI + 23.68 at 5° N and MEI + 25.27 at 5° S).

The correlation of the 0–5° N LER with the MEI is very high for major ENSO events in 1982–1983, 1986–1987, 1991–1992, and 1997–1998, and for most of the other later

ACPD
12, 31991–32038, 2012

significant ENSO events (e.g., 2010–2011). High correlations occur from 1979 to 2002, after which the correlation breaks down with an apparent anticorrelation in 2005 and 2008, during the period when ENSO occurred every year. The anticorrelation between the equatorial zonal mean LER and MEI can be attributed to the differences in spatial pattern between the Central Pacific types of ENSO (2004–2005, 2006–2007 El Nino) and the Eastern Pacific types of ENSO, 2005–2006 and 2007–2008 La Nina (Kao and Yu, 2009; Singh et al., 2011), with the positive correlation resuming in 2010. Over the period 1979 to 2011 the decadal pattern of variability of the MEI and LER are similar. For example, there is an apparent upward trend in the LER from 2000 to 2010 that also appears in the MEI. The matching of the long-term patterns between LER and MEI strongly suggests that the observed LER changes are not instrumental artifacts, but instead represent real physical changes in cloud plus aerosol reflectivity. A similar comparison for the zonal region 0–5° S shows a weaker 90-day correlation with MEI except for the two major ENSO events. However, the longer period (5 yr) correlation is apparent.

The volcanic eruptions from El Chichon (March 1982) and Mt. Pinatubo (June 1991) inserted large amounts of particulates into the atmosphere that were easily observable over a wide range of latitudes, especially at sunrise and sunset for a year after the eruptions. To see if these effects are in the LER time series, the annual cycle was removed from the 30° S to 30° N zonal average LER(30° S–30° N, t) time series by subtracting a best-fit sinusoid as a function of time (t, 0.5793, 0.50016 in years), $21.1327 - 0.6602\sin(\pi(t + 0.5793)/0.50016)$ RU. Figure 7 shows that the deseasonalized LER(30° S–30° N, t) short-term perturbations are coincident with major volcanic eruptions of El Chichon in 1982 and Mt. Pinatubo in 1991 as well as the major ENSO events represented by the MEI. However, a significant component of the MEI consists of local cloud observations that could also contain volcanic eruption perturbations. The effect of El Chichon and Mt. Pinatubo eruptions on the deseasonalized LER(30° S–30° N, t) cannot be clearly separated from the coincident ENSO events. In addition to the short term perturbations, the resulting deseasonalized time series has a long-term

ACPD
12, 31991–32038, 2012

linear decrease of 0.2 ± 0.01 RU per decade, which would be significant for estimating increases in solar insolation related to climate change.

6 Long-term change in LER

The long-term change in LER(θ,t) for each latitude band centered on θ can be estimated from a linear least squares fit to each zonal average LER time series or deseasonalized time series. Because of the length of the time series, and the use of complete years, the linear trend of each time series including the annual cycle and the deseasonalized time series are almost identical. The results (Fig. 8) show that there is a major difference in the LER change between the hemispheres. Most of the change occurs in the NH, having more land area compared to the SH, with more ocean area. There is also an additional large change in the equatorial region, $\theta = 15°$ S to 5° N that is caused by changes in the Pacific Ocean ENSO region near 175° W longitude. The largest change, $\Delta R = -0.9$ RU per decade, is near 50° N with large changes at 30° N–40° N ($\Delta R = -0.7$ RU per decade). A significant contribution comes from the equatorial band between 0° and 15° S ($\Delta R = -0.5$ RU per decade near the equator), which is important for estimating the change in energy reflected back to space caused by changes in the Earth's reflectivity.

To estimate the effect of reflectivity change on the energy reflected back to space, the zonally averaged LER(θ,t) is weighted by $\cos^2(\theta)$, to account for the decreasing area of higher latitude bands and for the angle of the incident solar irradiance for $\theta = 60°$ S to 60° N (Eq. 2 and Fig. 9). This simplified weighting neglects the small effect from the seasonal ±23.3° tilt of the Earth's rotation axis, which would introduce a 10 % annual cycle to the weighted LER(θ,t). A best fitting sin(t) function was subtracted from the data to provide a deseasonalized version (Fig. 9b). A linear least squares fit gives a decrease in the 60° S to 60° N reflectivity at a rate of 0.24 ± 0.01 RU per decade or a total of about 0.79 ± 0.03 RU since 1979. There are several multi-year cycles apparent

ACPD
12, 31991–32038, 2012

in the time series, including one near the end of the times series, indicating that the increase in LER above the least-squares mean during the past few years is temporary.

The average $\cos^2(\theta)$ weighted LER reflectivity (Eq. 2) for $\theta = 60^\circ$ S to 60° N is $\langle R \rangle$ = 26.9 RU for clouds plus aerosols and the Earth's surface. Of this amount, the average reflectivity of the surface is about 5 RU (estimated from Herman and Celarier, 1997), or $\langle R \rangle$ = 21.9 RU for clouds plus aerosols. The change over 33 yr is $\Delta\langle R \rangle = -0.24 \times 3.3 = -0.79$ RU. Assuming that there has been no long-term change in the surface reflectivity, the change (0.79 RU) represents a decrease of 3.6 ± 0.2 % of 340 nm energy reflected back to space by clouds plus aerosols over 33 yr.

$$\langle R \rangle = \frac{\sum\limits_{-60}^{60} \mathrm{LER}(\theta)\cos^2(\theta)}{\sum\limits_{-60}^{60} \cos^2(\theta)} \tag{2}$$

To estimate the effect of a 3.6 % decrease in cloud plus aerosol reflectivity in terms of shortwave energy change ΔE absorbed by the surface, we assume as starting values Trenberth et al. (2009) estimate of 341.3 W m^{-2} average solar energy at the top of the atmosphere, 78 W m^{-2} absorbed by the atmosphere, 79 W m^{-2} reflected by the atmosphere plus clouds and aerosols, and 23 W m^{-2} reflected by the surface (Fig. 10). Rayleigh scattering is assumed to be 6 % of the incident radiation or 4.74 W m^{-2}. Of the incoming radiation, 79 – 4.74 = 74.26 W m^{-2} are reflected by clouds and aerosols, giving a fractional cloud plus aerosol reflectivity of 74.26/341.3 = 0.2176. The estimated broadband reflectivity value is close to the fractional 340 nm LER estimate of $\langle R \rangle$ = 0.219. The radiation heading toward the surface is 341.3 – 78 – 79 = 184.3 W m^{-2}, of which 23 W m^{-2} is reflected from the surface yielding 102 W m^{-2} of total reflected radiation and 161.3 W m^{-2} absorbed by the surface. The effective fractional surface reflectivity based on Trenberth et al. is R_G = 23/184.3 = 0.1248, and is assumed to remain constant in time. For calculating energy change ΔE, the exact starting numbers

ACPD
12, 31991–32038, 2012

(i.e. Trenberth et al., 2009) do not make a significant difference. Extra significant figures are retained only for ease in checking the calculations.

Since the effects of Rayleigh scattering have been removed from the LER calculation (Eq. 1), it is assumed that the LER change measured at 340 nm can be applied over a wide wavelength range $\lambda < 1000\,nm$ containing about 70 % of the incident shortwave solar energy. To make a simplified calculation of the shortwave change ΔE in solar energy $\lambda < 4000\,nm$ (99 %) absorbed by the surface from change in reflectivity $\Delta\langle R\rangle$, it is assumed that the absorption of the atmosphere $78\,\mathrm{W\,m^{-2}}$ is constant in time out to 4000 nm.

Assuming the $78\,\mathrm{W\,m^{-2}}$ atmospheric absorption does not change with time, the 3.6 % decrease in average cloud plus aerosol reflectivity gives a reduced cloud plus aerosol fractional reflectivity of $0.2176 \times (1 - 0.036) = 0.2098$ giving $341.3 \times 0.2098 = 71.60\,\mathrm{W\,m^{-2}}$. Then the clouds and atmosphere reflect $71.60 + 4.74 = 76.34\,\mathrm{W\,m^{-2}}$, and $341.3 - 76.34 - 78 = 186.96\,\mathrm{W\,m^{-2}}$ reaches the surface. The amount reflected from the surface is now $23.33\,\mathrm{W\,m^{-2}}$ and $186.96 - 23.3 = 163.66\,\mathrm{W\,m^{-2}}$ is absorbed by the surface. The total reflected solar radiation is now $76.34 + 23.33 = 99.67\,\mathrm{W\,m^{-2}}$. The difference is $99.67 - 102 = -2.33\,\mathrm{W\,m^{-2}}$, which is the same as the difference absorbed by the surface, $\Delta E = 163.63 - 161.3 = 2.33\,\mathrm{W\,m^{-2}}$, or a change of 1.4 %.

The net change in shortwave radiation absorbed by the surface, $\Delta E = 2.3\,\mathrm{W\,m^{-2}}$, is partially offset by a change in longwave cooling to space arising from the decrease in cloud plus aerosol amount, an increase in thermal energy radiated at the surface caused by a 0.5 °C increase in global average surface temperature since 1979 (Hansen et al., 2009), and changes in tropospheric temperatures. The amount of the longwave offset plus changes in atmospheric absorption determine whether the cloud plus aerosol change represents a positive or negative feedback.

Including the seasonal change in insolation (solar declination changing between ±23.3°), starting with $1361\,\mathrm{W\,m^{-2}}$ at the top of the atmosphere (TOA) and the noontime-corrected latitude by longitude 340 nm LER for each day since 1979 (Fig. 11) modified by the average diurnal LER variation (Labow et al., 2011), we obtain a nearly

ACPD
12, 31991–32038, 2012

identical value of 2.28 $W m^{-2}$ increase in solar radiation absorbed by the earth's surface over 33 yr.

As shown in Fig. 10, the long-term decreases in LER(θ,φ,t) mostly occur over land in both the SH and NH, with the largest LER decreases occurring over Central Europe. The results suggest a gradual increase in solar energy reaching the ground and long-wave cooling to space since 1979 for these regions. In contrast with LER decreases over adjacent land areas, the LER change over the nearby Pacific Ocean ranges from local increases to areas where the changes are statistically not different from zero. The clear separation for ΔLER(θ,φ) between land and ocean indicates that the observed zonal average LER decreases are not from the SBUV and SBUV/2 calibration issues. The decrease of cloud cover from Eastern Asia over the Pacific Ocean largely dissipates before reaching the middle of the Pacific Ocean. The same is not the case over the much smaller Northern Atlantic Ocean, where the prevailing west to east winds transport continental cloud cover over the ocean. This means that the decreases in cloud amount over the Northern US and Canada can also be seen over the North Atlantic.

The noon normalized time correction (Labow et al., 2011) could not be applied at high latitudes above 60° in (Fig. 10 lower panel) because of insufficient diurnal data from the satellites. In both the uncorrected and noon normalized data there has been no change observed over most of Central Africa, with a small decrease in LER over South Eastern Africa near Madagascar. The land regions showing the largest LER increase are in India and Indochina. Australia and New Zealand are largely unchanged. North and South America show a significant decrease in LER. There are interesting ΔLER(θ,φ) features over the oceans that are related to clouds that appear to be associated with ocean currents. Cloud cover has increased over the region where the Humboldt Current impacts the western coast of South America in the region between 10° S and 20° S. There is a similar increase off the west coast of North America associated with the California Current and in the Pacific region just north of the Equator at 5° N and a large region of decrease just south of the equator near 170° W to 170° E. The regions of LER

ACPD
12, 31991–32038, 2012

A net decrease in the Earth's cloud plus aerosol reflectivity 1979–2011

J. R. Herman et al.

increase near the west coasts of North and South America also appear as regions of enhanced cloud cover in Fig. 2. A smaller, but similar feature appears near Indonesia and runs southward to just northeast of Australia.

Most of the estimated change in solar insolation comes from the latitude bands between 15° S to 0° (31 %) and between 25° N to 60° N (36.3 %). The percent distribution of solar insolation increase with latitude is shown in Fig. 12. If the LER changes are caused by global warming, then the LER change may represent a positive feedback that amplifies the warming effect over land in the NH, parts of the SH, and the north polar region (Fig. 11). In the Arctic region, the LER data are entirely from April to August, so that the trends shown near the Arctic in Fig. 11 are representative of the summer months. Since the maximum amounts of daily solar insolation occurs at latitudes poleward from the Arctic (and Antarctic) circle during summer, long-term decreases in LER (increases in solar insolation) may contribute to decreasing ice amounts. However, the LER cannot separate decreases in ice reflectivity from decreases in cloud reflectivity. If the observed LER decreases are partly caused by areal decreases in ice reflectivity, the change still represents less energy reflected back to space and more solar energy absorbed by the surface.

7 Regional LER time series and trends

7.1 Mid Pacific Ocean

Figure 13 shows a 90-day low pass filter LER time series (black) for a portion of this region bounded by the box 1° S–9° S, 157° W–177° W along with the MEI (grey) showing a degree of correlation for most LER events. The correlations with MEI are similar to those in Fig. 6 except that the local LER decreases (2 ± 0.1 RU decade^{-1}) are much larger than for the equatorial zonal average (0.5 RU decade^{-1}).

The time series appears to be dominated by peaks occurring in 1983, 1987, 1992, and 1998, which could affect the estimated linear slope. The MEI time series also has a

ACPD
12, 31991–32038, 2012

slope of -0.2 ± 0.05 per decade. After removing the slope from the multivariate ENSO Index to obtain MEI_D, and then creating the function $LER_D = LER - 4MEI_D + 19.47$, the major peaks are removed and the new slope estimated as -2.1 ± 0.1 per decade, which is approximately the same as before. Figures 11 and 13 suggest that there is a long-term change in the underlying ocean currents in the equatorial region and a decrease in the frequency of major ENSO events. The larger peaks in LER and MEI after 2000 (2003 and 2010) are significantly smaller than the four earlier peaks. The decrease in LER during the past three decades (Fig. 12) is consistent with the observed decrease in equatorial precipitation and cloud cover in the Central Pacific (0 to 10° S, 150° E to 120° W) during 1979 to 2010 (Gu and Adler, 2011).

8 Additional sites

LER trends from additional specific sites selected from regions with significant change shown in Fig. 11 are shown in Figs. 14 to 16 and Table 2 along with maps Figs. 14–16 taken from Google Earth.

8.1 South America

The same multi-year patterns appear in the South American LER time series with opposite trends over the ocean and over land (Fig. 14). The trend over land is similar to those on North America (Table 2).

8.2 Greenland

The LER trend over Greenland (Fig. 15) shows that a significant decrease in scene reflectivity may be partly composed of changes in surface ice reflectivity or changes in the cloud cover over the ice. For ice-covered scenes, the situation is uncertain, since clear-sky scenes are brighter than clouds over ice. However, the adjacent areas show decreased reflectivity over the nearby oceans, suggesting that more sunlight is reach-

ACPD
12, 31991–32038, 2012

ing the ice surface, causing it to darken because of melting. Most of the data shown in Fig. 15 is from the summer because of the high latitude, where sunlight to disappears after the September equinox.

8.3 India, Southern China, and Indochina

There is an increase in LER of 0.5 RU decade^{-1} over a wide region indicated by the box drawn in Fig. 16 that implies a decrease in sunlight reaching the surface. Specific areas within this region (e.g. Southern India, Table 2) have larger increasing trends (0.89 RU decade^{-1}) than the area average. The increasing LER is consistent with the observed increase in rainfall in the Asian monsoon region (Gu and Adler, 2011).

8.4 LER Trends at Various Locations

Table 2 contains a list of LER trends at various locations shown in Fig. 17.

9 Summary

This study shows that a consistent calibration and common retrieval algorithm applied to seven SBUV instruments over three decades is sufficient to detect long-term changes in cloud plus aerosol reflectivity that can be differentiated from seasonal or instrumental differences. This is partly demonstrated by the comparison of the LER with the Mulitvariate ENSO Index (MEI), which showed high correlation for the larger ENSO events in 1982–1983 and 1991–1992. The estimated trends in LER are a function of location, with little or no trend over the Pacific Ocean adjacent to the decreasing LER trend over North America. The clear difference between adjacent land and ocean areas shows that the trends are neither instrument artifacts nor incorrect calibrations over the 33-yr period. The 60° S to 60° N change in cosine^2(Latitude) weighted LER, which is used for approximating changes in energy reflected back to space from changes in LER, shows a global average increase in the amount of solar energy reaching the

Discussion Paper | Discussion Paper | Discussion Paper | Discussion Paper |

ACPD

12, 31991–32038, 2012

A net decrease in the Earth's cloud plus aerosol reflectivity 1979–2011

J. R. Herman et al.

surface of 2.7 $W m^{-2}$ and, using the energy partitioning from Trenberth et al. (2009), an estimated increase in energy absorbed by the surface and decrease of energy reflected back to space of 2.3 $W m^{-2}$ or a 1.4 % change. This average change is unevenly distributed as a function of latitude and longitude, with the largest decreases in LER occurring over land in the NH and over the North Atlantic Ocean (including Greenland). There are significant areas over India, Southern China, and Indochina where the LER has increased (decreased insolation), a large increase on the west coast of South America that is in the region where the Humboldt current impacts the South American continent (Peru and Chile), and a large decrease in LER in the equatorial mid-Pacific Ocean near 170° W to 10° E longitude. The decrease in LER is consistent with an increase in surface solar radiation reaching the Earth's surface, which was also observed in the global surface radiation network (Wild et al., 2005; Pinker et al., 2005).

Acknowledgements. This research is supported by the NASA MEaSUREs Project. The data and documentation are available at the GES-DISC (http://daac.gsfc.nasa.gov/).

References

Ahmad, Z., DeLand, M. T., Cebula, R. P., Weiss, H., Wellemeyer, C. G., Planet, W. G., Lienesch, J. H., Bowman, H. D., Miller, A. J., and Nagatani, R. M.: Accuracy of total ozone retrieval from NOAA SBUV/2 measurements: impact of instrument performance, J. Geophys. Res., 99, 22975–22984, 1994.

Burgman, R. J., Clement, A. C., Mitas, C. M., Chen, J., and Esslinger, K.: Evidence for atmospheric variability over the Pacific on decadal timescales, Geophys. Res. Lett., 35, L01704, doi:10.1029/2007GL031830, 2008.

Chandrasekar, S.: Radiation Transfer, Oxford Clarendon Press, New York: Dover, ISBN 0-486-60590-6, 1960

Chen, J., Del Genio, A. D., Carlson, B. E., and Bosilovich, M. G.: The spatiotemporal structure of twentieth-century climate variations in observations and reanalyses, Part I: long-term trend, J. Clim., 21, 2611–2633, 2008.

DeLand, M. T., Cebula, R. P., Huang, L.-K., Taylor, S. L., Stolarski, R. S., and McPeters, R. D.: Observations of hysteresis in backscattered ultraviolet ozone data, J. Atmos. Ocean. Tech., 18, 914–924, 2001.

DeLand, M. T., Taylor, S. L., Huang, L. K., and Fisher, B. L.: Calibration of the SBUV version 8.6 ozone data product, Atmos. Meas. Tech. Discuss., 5, 5151–5203, doi:10.5194/amt-5-2951-2012, 2012.

Dobber, M., Q. Kleipool, R. Dirksen, P. Levelt, G. Jaross, S. Taylor, T. Kelly, L. Flynn, G. Leppelmeier, and Rozemeijer, N.: Validation of ozone monitoring instrument level 1b data products, J. Geophys. Res., 113, D15S06, doi:10.1029/2007JD008665, 2008.

Evan, A. T., Heidinger, A. K., and Vimont, D. J.: Arguments against a physical long-term trend in global ISCCP cloud amounts, Geophys. Res. Lett., 34, L04701, doi:10.1029/2006GL028083, 2007.

Fegley, A. A. and Fowler, W. K.: Radiometric calibration of SBUV/2 instruments: retrospective improvements, Metrologia, 28, 297–300, 1991.

Frederick, J. E., Cebula, R. P., and Heath, D. F.: Instrument characterization for the detection of long-term changes in stratospheric ozone: an analysis of the SBUV/2 radiometer, J. Atmos. Oceanic Technol., 3, 472–480, 1986.

Georgiev, G. T. and Butler, A. A.: Long-term calibration monitoring of spectralon diffusers BRDF in the air-ultraviolet, Appl. Opt. 46, 7892–7899, 2007.

Gu, G. and Adler, R. F.: Interdecadal variability/long-term changes in global precipitation patterns during the past three decades: global warming and/or Pacific decadal variability?, Clim. Dynam., doi:10.1007/s00382-012-1443-8, in press, 2012.

Hansen, J., Ruedy, R., Sato, M., and Lo, K.: Global surface temperature change, Rev. Geophys., 48, RG4004, doi:10.1029/2010RG000345, 2010.

Hansen, J., Sato, M., Kharecha, P., and von Schuckmann, K.: Earth's energy imbalance and implications, Atmos. Chem. Phys., 11, 13421–13449, doi:10.5194/acp-11-13421-2011, 2011.

Hartmann, D. L., Ockert-Bell, M. E., and Michelsen, M. L.: The effect of cloud type on earth's energy balance: global analysis, J. Climate, 5, 1281–1304, 1992.

Haynes, J. M., Jakob, C., Rossow, W. B., Tselioudis, G., and Brown, J.: Major characteristics of Southern Ocean cloud regimes and their effects on the energy budget, J. Climate, 24, 5061–5080, doi:10.1175/2011JCLI4052.1, 2011.

Heath, D. F., Mateer, C. L., and Kreuger, A. J.: The Nimbus-4 BUV atmospheric ozone experiment – two year's operation, Pure Appl. Geophys., 106, 1238–1253, 1973.

Heath, D. F., Krueger, A. J., Roeder, H. A., and Henderson, B. D.: The solar backscatter ultraviolet and total ozone mapping spectrometer (SBUV/TOMS) for Nimbus G, Opt. Eng., 14, 323–331, 1975.
Herman, J. R.: Changes in ultraviolet and visible solar irradiance 1979 to 2008, in: UV Radiation in Global Change: Measurements, Modeling and Effects on Ecosystems, edited by: Gao, W., Schmoldt, D., and Slusser, J., Springer Heidelberg Dordrecht London New York, ISBN 978-3-642-03312-4, 2009.
Herman, J. R.: Global increase in UV irradiance during the past 30 yr (1979–2008) estimated from satellite data, J. Geophys. Res., 115, D04203, doi:10.1029/2009JD012219, 2010.
Herman, J. R. and Celarier, E. A.: Earth surface reflectivity climatology at 340 nm to 380 nm from TOMS data, J. Geophys. Res., 102, 28003–28011, 1997.
Herman, J. R., Celarier, E., and Larko, D.: UV 380 nm reflectivity of the Earth's surface, clouds, and aerosols, J. Geophys. Res., 106, 5335–5351, 2001.
Herman, J. R., Labow, G., Hsu, N. C., and Larko, D.: Changes in cloud cover (1998–2006) derived from reflectivity time series using SeaWiFS, N7-TOMS, EP-TOMS, SBUV-2, and OMI radiance data, J. Geophys. Res., 114, D01201, doi:10.1029/2007JD009508, 2009.
Hilsenrath, E., Cebula, R. P., DeLand, M. T., Laamann, K., Taylor, S., Wellemeyer, C., and Bhartia, P. K.: Calibration of the NOAA 11 SBUV/2 ozone data set from 1989 to 1993 using in-flight calibration data and SSBUV, J. Geophys. Res., 100, 1351–1366, 1995.
Huang, L.-K., Cebula, R. P., and Hilsenrath, E.: New procedure for interpolating NIST FEL lamp irradiances, Metrologia, 35, 381–386, 1998.
Huang, L.-K., Cebula, R. P., Taylor, S. L., DeLand, M. T., McPeters, R. D., and Stolarski, R. S.: Determination of NOAA-11 SBUV/2 radiance sensitivity drift based on measurements of polar ice cap radiance, Int. J. Remote Sens., 24, 305–314, 2003.
IPCC (Intergovernmental Panel on Climate Change): Climate Change 2007: The Physical Science Basis, Cambridge University Press, Cambridge, UK, 2007.
Janz, S., Hilsenrath, E., Butler, J., Heath, D. F., and Cebula, R. P.: Uncertainties in radiance calibrations of backscatter ultraviolet (BUV) instruments, Metrologia, 32, 637–641, 1995.
Jaross, G. and Warner, J.: Use of Antarctica for validating reflected solar radiation measured by satellite sensors, J. Geophys. Res., 113, D16S34, doi:10.1029/2007JD008835, 2008.
Kao, H.-Y. and Yu, J.-Y.: Contrasting Eastern-Pacific and Central-Pacific types of ENSO, J. Climate, 22, 615–632, 2009.

ACPD
12, 31991–32038, 2012

A net decrease in the Earth's cloud plus aerosol reflectivity 1979–2011

J. R. Herman et al.

Kiehl, J. T. and Trenberth, K. E.: Earth's annual global mean energy budget, B. Am. Meteorol. Soc., 78, 197–208, 1997.
Kleipool, Q. L., Dobber, M. R., de Haan, J. F., and Levelt, P. F.: Earth surface reflectance climatology from 3 yr of OMI data, J. Geophys. Res., 113, D18308, doi:10.1029/2008JD010290, 2008.
Kopp, G. and Lean, J. L.: A new, lower value of total solar irradiance: evidence and climate significance, Geophys. Res. Lett., 38, L01706, doi:10.1029/2010GL045777, 2011.
Labow, G. J., Herman, J. R., Huang, L.-K., Lloyd, S. A., DeLand, M. T., Qin, W., Mao, J., and Larko, D. E.: Diurnal variation of 340 nm Lambertian equivalent reflectivity due to clouds and aerosols over land and oceans, J. Geophys. Res., 116, D11202, doi:10.1029/2010JD014980, 2011.
Norris, J. R. and Slingo, A.: Trends in observed cloudiness and Earth's radiation budget: what do we not know and what do we need to know? in: Clouds in the Perturbed Climate System, edited by: Heintzenberg, J. and Charlson, R. J., MIT Press, 17–36, 2009.
O'Byrne, G., Martin, R. V., van Donkelaar, A., Joiner, J., and Celarier, E. A.: Surface reflectivity from the ozone monitoring instrument using the moderate resolution imaging spectroradiometer to eliminate clouds: effects of snow on ultraviolet and visible trace gas retrievals, J. Geophys. Res., 115, D17305, doi:10.1029/2009JD013079, 2010.
Pinker, R. T., Zhang, B., and Dutton, E. G.: Do satellites detect trends in surface solar radiation?, Science, 308, 850–854, doi:10.1126/science.1103159, 2005.
Rossow, W. B. and Schiffer, R. A.: Advances in understanding clouds from ISCCP, Bull. Amer.Meteor. Soc., 80, 2261–2287, 1999.
Schiffer, R. A. and Rossow, W. B.: The international satellite cloud climatology project (ISCCP): the first project of the World Climate Research programme, B. Am. Meteorol. Soc., 64, 779–784, 1983.
Schlesinger, B. M. and Cebula, R. P.: Solar variation 1979–1987 estimated from an empirical model for changes with time in the sensitivity of the solar backscatter ultraviolet instrument, J. Geophys. Res., 97, 10119–10134, 1992.
Singh, A., Delcroix, T., and Cravatte, S.: Contrasting the flavors of El Nino Southern Oscillation using sea surface salinity observations, J. Geophys. Res., 116, C06016, doi:10.1029/2010JC006862, 2011.
Stevens, B. and Schwartz, S. E.: Observing and modeling Earth's energy flows, Surveys Geophys., 33, 779–816, doi:10.1007/s10712-012-9184-0, 2012.

Trenberth, K. E., Fasullo, J. T. and Kiehl, J.: Earth's global energy budget, B. Am. Meteorol. Soc., 90, 311–324, doi:10.1175/2008BAMS2634.1, 2009.
Veefkind, J. P., de Haan, J. F., Brinksma, E. J., Kroon, M., and Levelt, P. F.: Total ozone from the ozone monitoring instrument (OMI) using the DOAS technique, IEEE T. Geosci. Remote, 44, 1239–1244, 2006.
Weiss, H., Cebula, R. P., Laamann, K., and Hudson, R. D.: Evaluation of the NOAA 11 solar backscatter ultraviolet radiometer, mod 2 (SBUV/2): inflight calibration, Proc. SPIE Int. Soc. Opt. Eng., 1493, 80–90, 1991.
Wild, M., Gilgen, H., Roesch, A., Ohmura, A., Long, C. N., Dutton, E. G., Forgan, B., Kallis, A., Russak, V., and Tsvetkov, A.: From dimming to brightening: decadal changes in solar radiation at Earth's surface, Science, 308, 847–850, doi:10.1126/science.1103215, 2005.
Wolter, K. and Timlin, M. S.: Monitoring ENSO in COADS with a seasonally adjusted principal component index, Proc. of the 17th Climate Diagnostics Workshop, Norman, OK, NOAA/NMC/CAC, NSSL, Oklahoma Clim. Survey, CIMMS and the School of Meteor., University of Oklahoma, Norman, Oklahoma, USA, 52–57, 1993.
Wolter, K. and Timlin, M. S.: Measuring the strength of ENSO events – how does 1997/98 rank?, Weather, 53, 315–324, 1998.
Wylie, D., Jackson, D. L., Menzel, W. P., and Bates, J. J.: Trends in global cloud cover in two decades of HIRS observations, B. Am. Meteorol. Soc., 18, 3021–3031, 2005.

Table 1. UV Satellite Data Sets Used for 340 nm LER.

1978–1990	Nimbus-7/SBUV	340 nm reflectivity is produced as part of standard processing using a new Antarctic ice radiance in-flight calibration. 14 nadir viewing orbits per day. Full global coverage once per week. Only a few missing days. Near noon Sun-synchronous orbit.
1985–2006	NOAA SBUV/2 Series 9, 11, 14	340 nm reflectivity is produced as part of standard processing using a new Antarctic ice radiance in-flight calibration. There are 14 nadir viewing orbits per day giving full global coverage once per week with only a few missing days. The equator crossing times drifted during the instrument's lifetime. A small time of day correction has been applied.
2004–present	OMI	340 nm daily reflectivity is now part of standard processing using pre-flight and in-flight calibration. Very stable instrument. Full global coverage every day. Reflectivity values are available for all wavelengths from 330 nm to 500 nm for a 13:30 Sun synchronous orbit. However, there is an offset between the UV2 (300–370 nm) and VIS (350–500 nm) detectors. Adding OMI to the SBUV SBUV/2 340 nm time series does not alter the estimate of long-term change in LER.
2002–present	NOAA-SBUV-2 series 16, 17, 18, 19	340 nm daily reflectivity using a new Antarctic ice radiance in-flight calibration. There are 14 nadir viewing orbits per day giving full global coverage once per week with only a few missing days. Near noon Sun synchronous orbit for the first 5 yr.

Table 2. LER Trends at Locations in Fig. 17.

Location Name	Latitude	Longitude	LER Trend ($\mathrm{RU\,Decade^{-1}}$)
Europe	45° N to 51° N	7.5° E to 17.5° E	−1.35
United States	31° N to 49° N	117.5° W to 82.5° W	−0.97
Canada	49° N to 53° N	127.5° W to 72.5° W	−0.38
Madagascar	19° S to 13° S	42.5° E to 47.5° E	−1.14
Atlantic West of Africa	25° S to 13° S	2.5° W to 2.5° E	+0.64
Southern India	11° N to 19° N	72.5° E to 77.5° E	+0.89
Equatorial Pacific Ocean	1° S to 9° S	157° W to 177° W	+2.1
South America Land	11° S to 29° S	42.5° W to 67.5° W	−0.9
South America Ocean	11° S to 29° S	82.5° W to 102.5° W	+0.8
South East Asia	11° N to 29° N	72.5° E to 112.5° E	+0.5
Greenland	71° N to 75° N	37.5° W to 42.5° W	−0.3

ACPD
12, 31991–32038, 2012

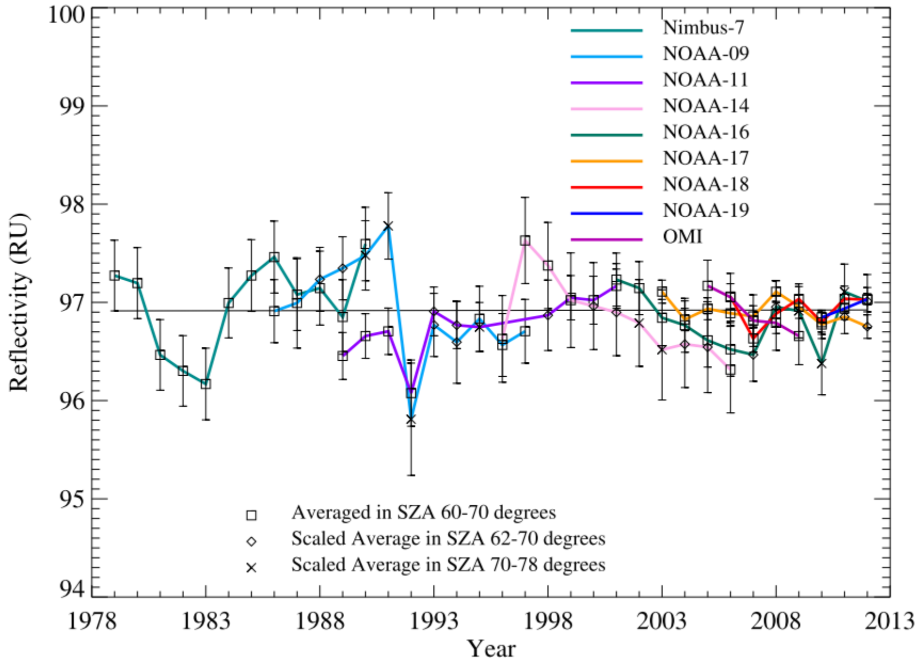

Fig. 1. Normalized summer Antarctic snow/ice LER at 340 Δ1.1 *nm* averaged between SZA 60° to 70°. Squares: LER averaged over 60° < SZA < 70°. Diamonds: LER averaged over 62° < SZA < 70°. X: LER averaged over 70° < SZA < 78° and interpolated from the first year of data back to the range LER averaged over 60° < SZA < 70°. The average LER for each satellite is adjusted to 96.92 RU based on the best calibrated 4 SBUV/2 instruments. The "error bars" are a combination the standard deviation of the envelope of values and the annual deviation from the mean.

ACPD
12, 31991–32038, 2012

ACPD
12, 31991–32038, 2012

A net decrease in the Earth's cloud plus aerosol reflectivity 1979–2011

J. R. Herman et al.

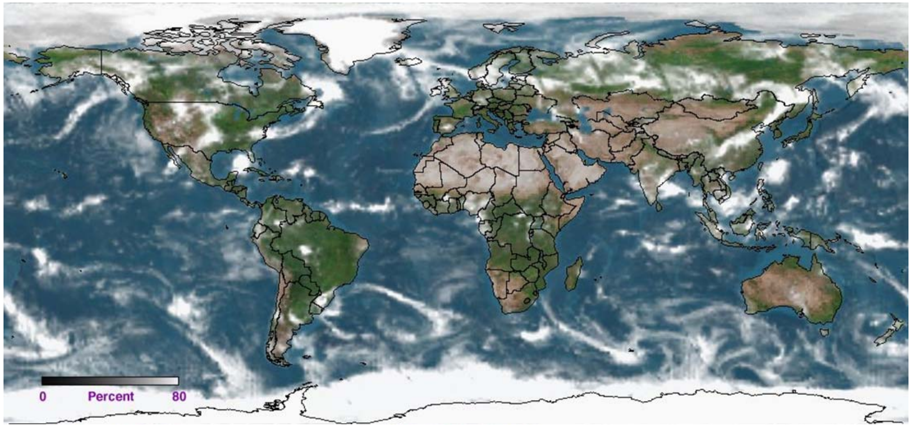

Fig. 2. The 340 Δ1.1 *nm* LER from AURA/OMI for 10 September 2008. The hurricane in the Gulf of Mexico is a Category 4 Hurricane named Ike. The LER (black, grey, and white, scale lower left) is superimposed on a MODIS clear-sky color map.

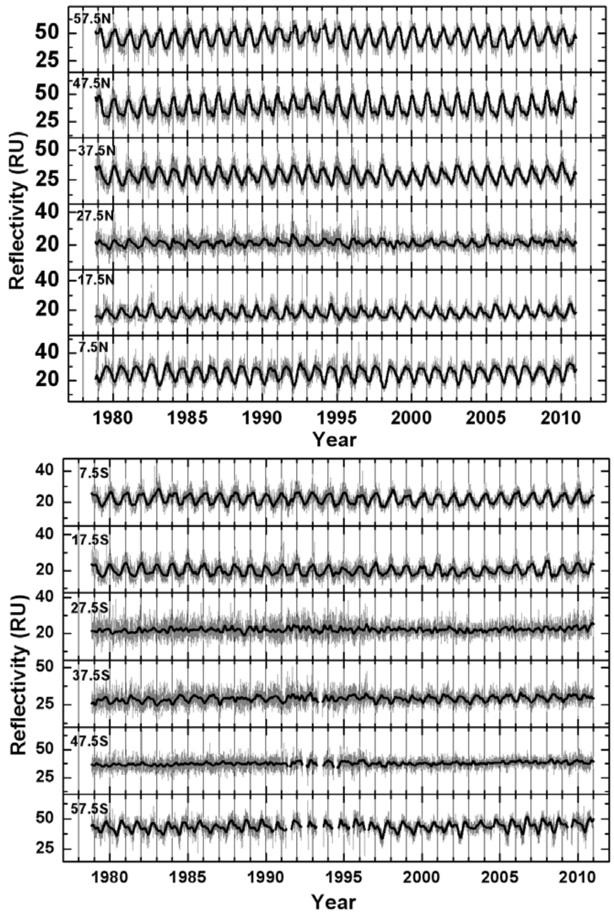

Fig. 3. LER zonal average time series for twelve 5° bands from 57.5° S to 57.5° N (1979–2010). The light grey color corresponds to daily LER, while the black solid lines are a 30-day low-pass filter of the daily data.

ACPD
12, 31991–32038, 2012

A net decrease in the Earth's cloud plus aerosol reflectivity 1979–2011

J. R. Herman et al.

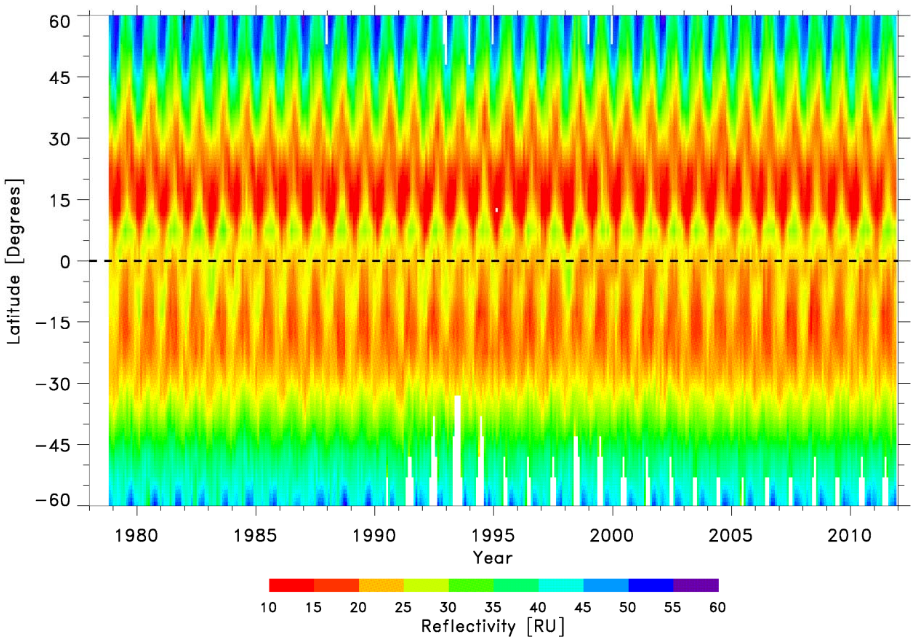

Fig. 4. Zonal mean monthly averages of LER 1979–2011 for latitudes between 60° S to 60° N showing the seasonal patterns as a function of latitude. White is missing data.

ACPD
12, 31991–32038, 2012

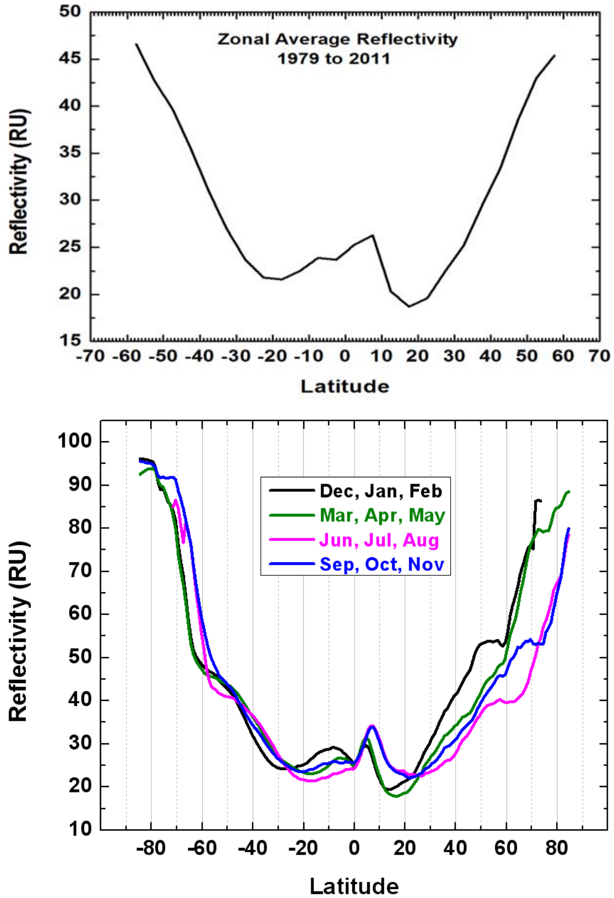

Fig. 5. (Upper) Thirty-three year average of the zonal average time series as a function of latitude from the SBUV series of instruments. (Lower) Four year seasonal average of OMI LER data (black: December–February, green: March–May, magenta: June–August, blue: September–November).

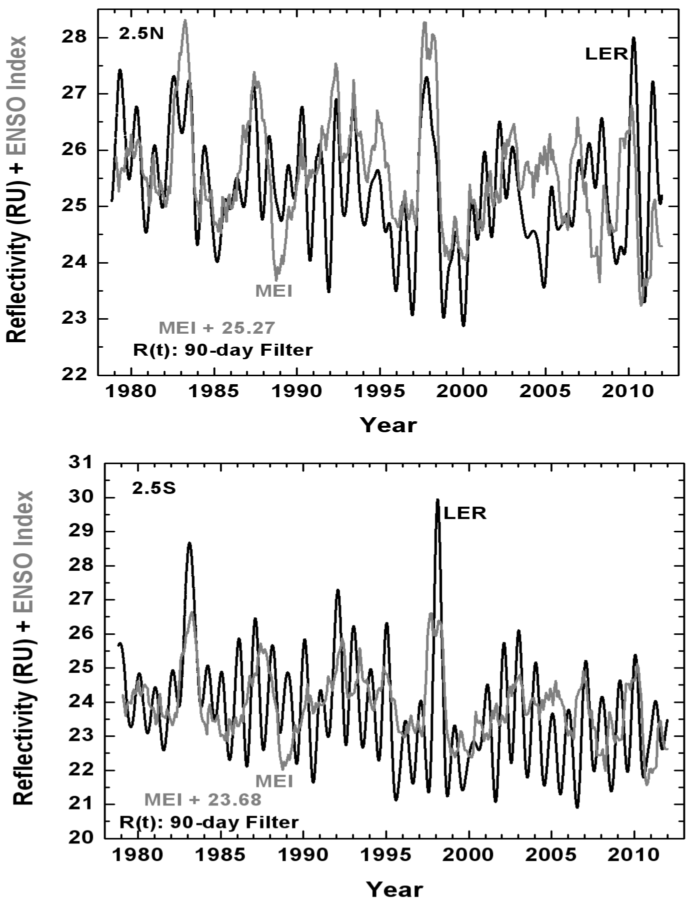

Fig. 6. A comparison of the LER (black) with the scaled MEI + R_{AVG} (grey) for the latitude bands 0 to 5° N (top) and 0 to 5° S (bottom). The LER is a 90-day low pass filter of the daily LER time series.

ACPD
12, 31991–32038, 2012

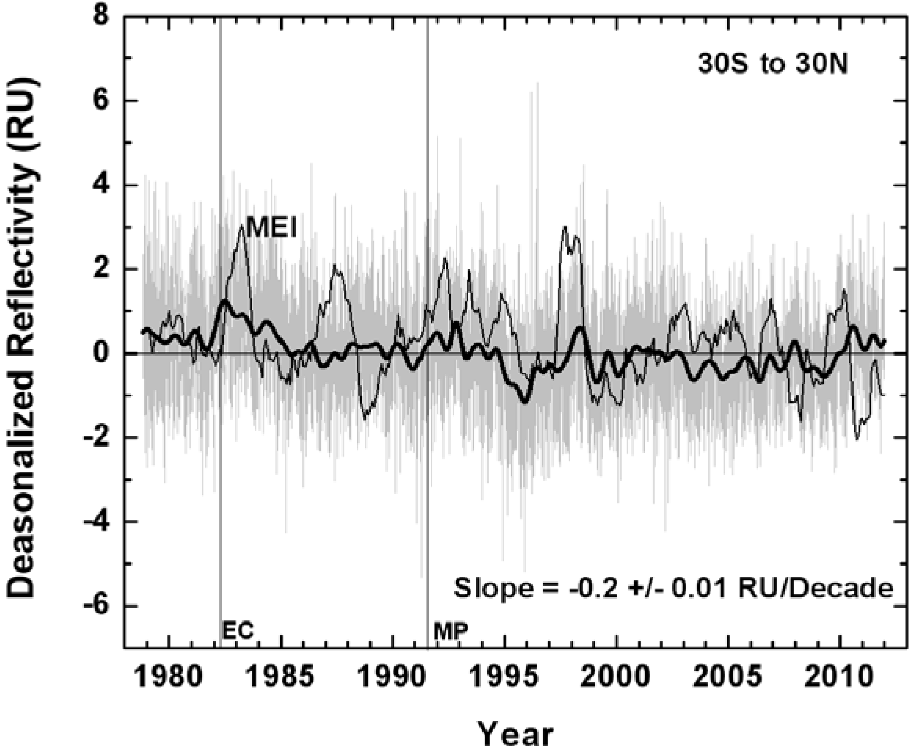

Fig. 7. Deseasonalized LER time series for 30° S to 30° N (grey) with a superimposed 90-day low-pass filter (thick black) and the MEI (thin black). The lines labeled EC and MP represent the dates of the El Chichon (April 1982) and Mt. Pinatubo (June 1991) volcanic eruptions.

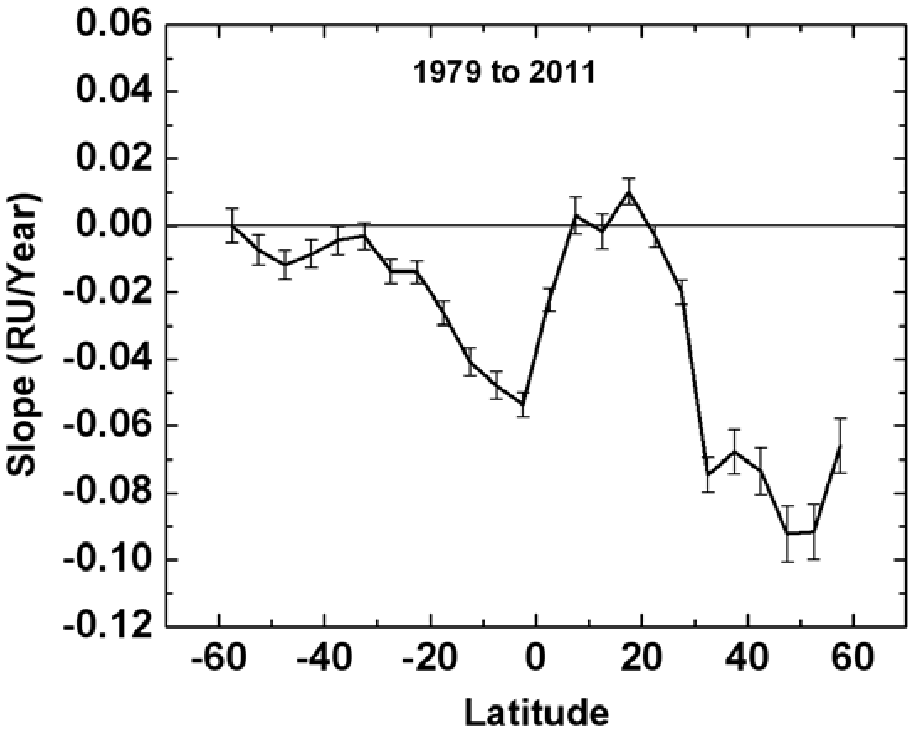

Fig. 8. Zonal average trends ($RU\,yr^{-1}$) 1979 to 2011.

ACPD
12, 31991–32038, 2012

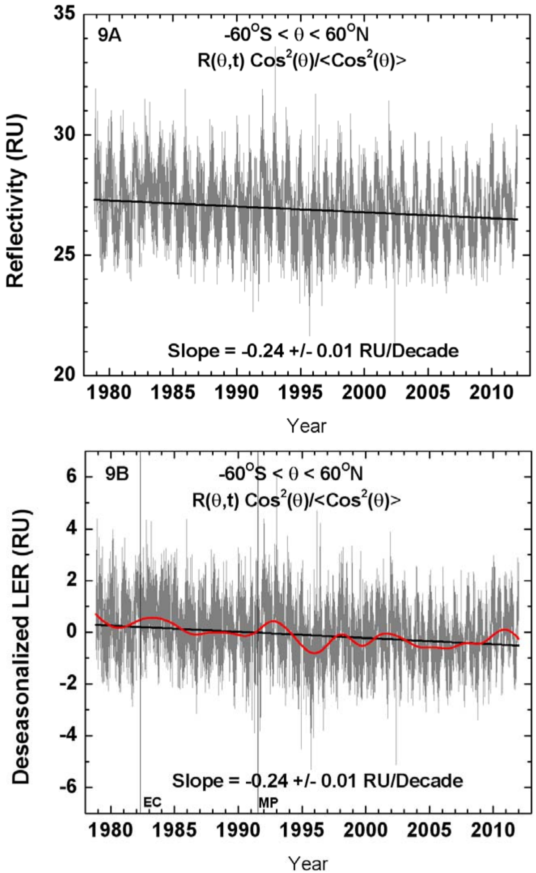

Fig. 9. (A) Normalized $\cos^2(\theta)$ weighted zonal average reflectivity for $\theta = 60^\circ$ S to 60° N, **(B)** Normalized deseasonalized LER(θ,t) $\cos^2(\theta)$ for $\theta = 60^\circ$ S to 60° N. The dark solid line is a 365-day low pass filter showing the major multi-year cycles. Normalization $\langle \cos^2(\theta) \rangle = 0.707$. EC = El Chichon and MP = Mt. Pinatubo.

ACPD
12, 31991–32038, 2012

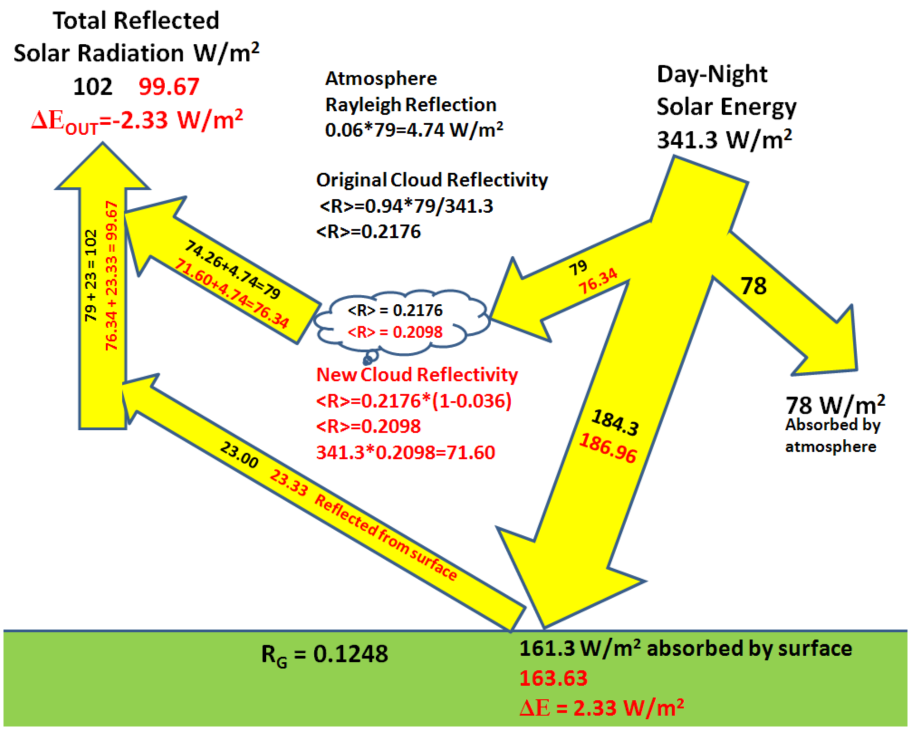

Fig. 10. Shortwave energy balance diagram based on Trenberth et al. (2009). The numbers in black are from Trenberth. The numbers in red are from the effect of changing the cloud + aerosol reflectivity $\langle R \rangle$ by 3.6 % from Trenberth's implied value of 21.76 RU to 20.98 RU. The result is an increase of 1.4 % in energy absorbed by the surface.

ACPD
12, 31991–32038, 2012

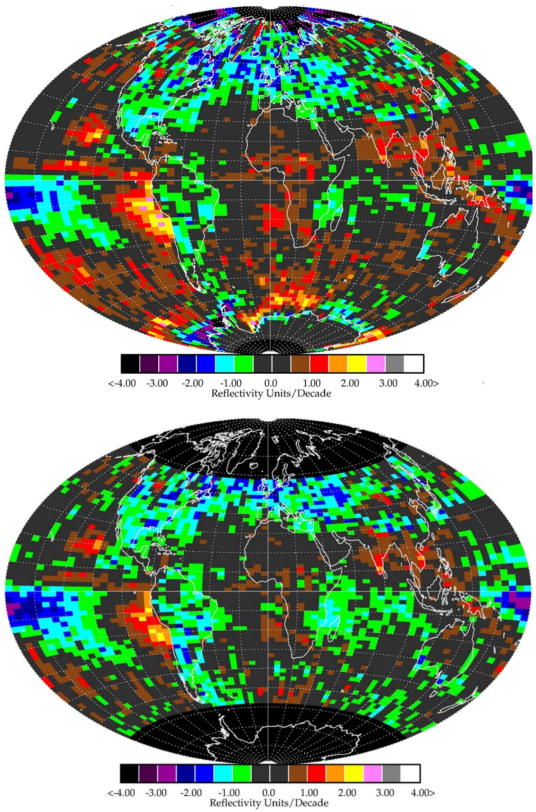

Fig. 11. LER linear trends ΔLER(θ,φ) as a function of latitude θ and longitude φ. The upper graph has no time correction applied to the data, while the lower graph is based on LER normalized to noon. The noon normalization could not be applied to latitudes $> 60^\circ$ because of a lack of measured radiances at different local times.

ACPD
12, 31991–32038, 2012

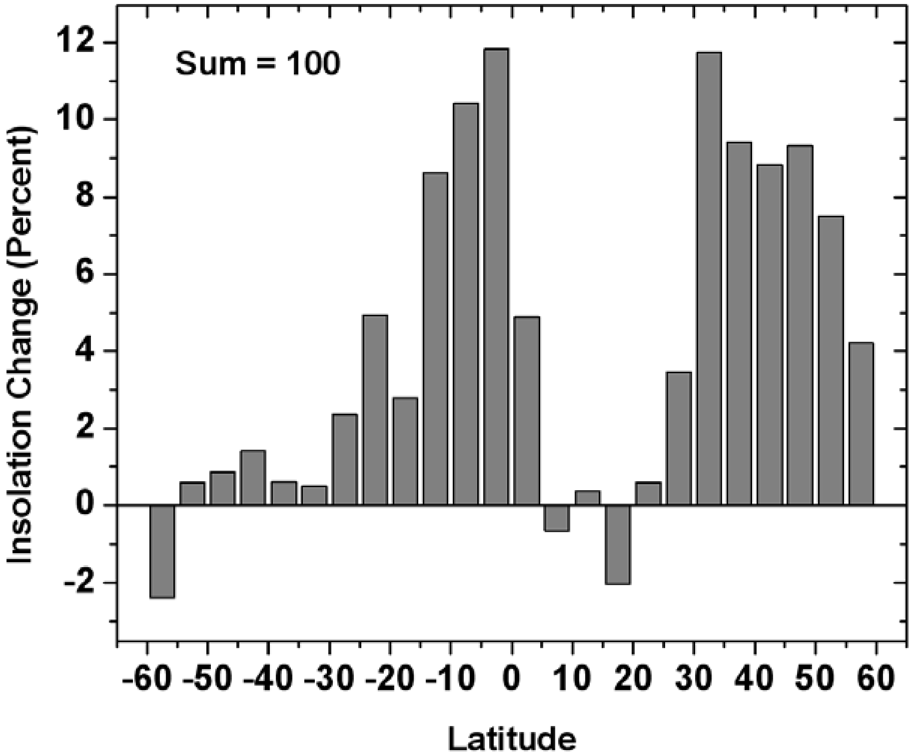

Fig. 12. Percent change in solar insolation as a function of latitude normalized to sum to 100.

ACPD
12, 31991–32038, 2012

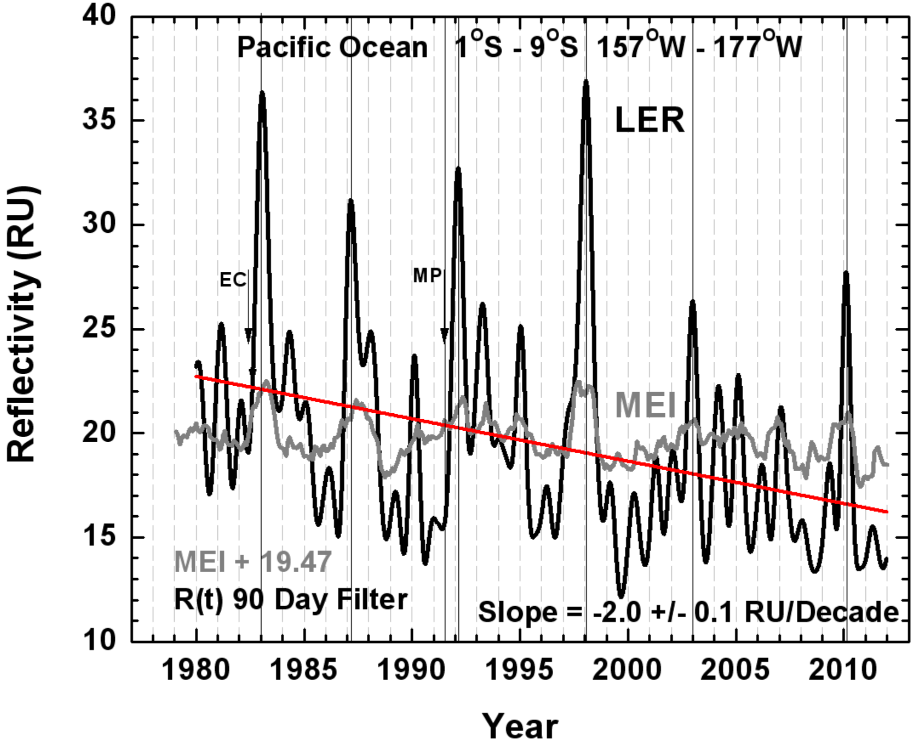

Fig. 13. LER time series (black) compared with the offset MEI + 19.47 (grey) for the Pacific region shown in Fig. 8 with large reflectivity change.

ACPD
12, 31991–32038, 2012

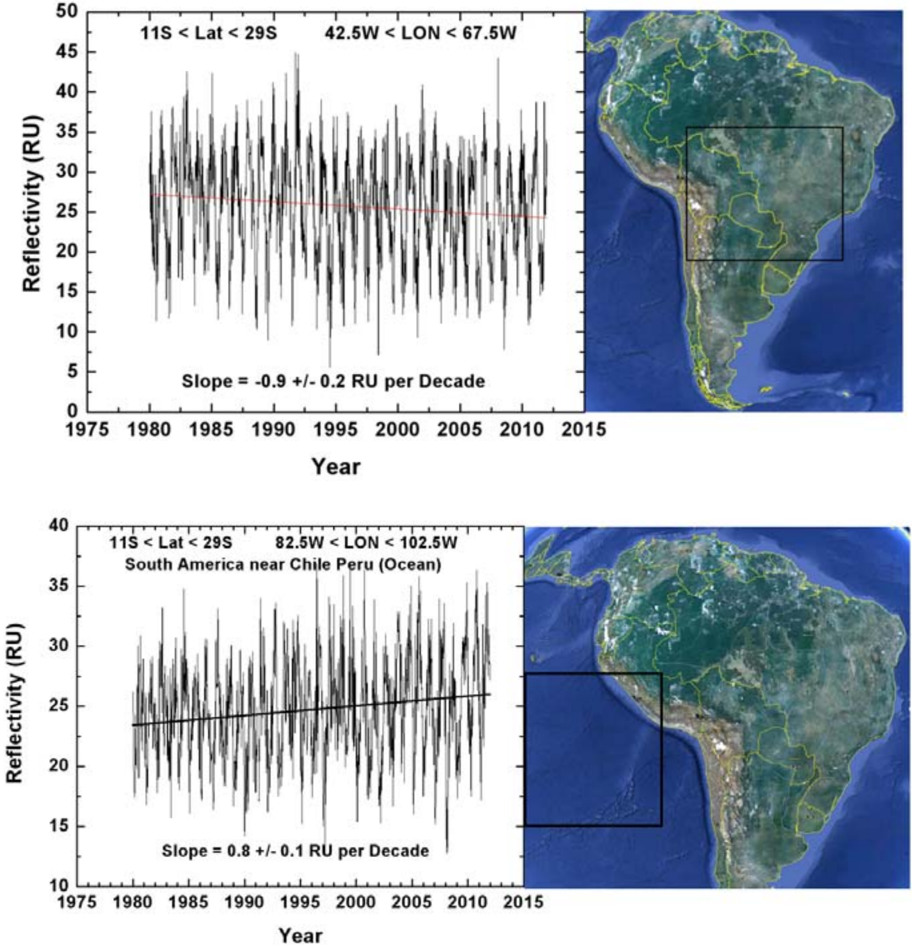

Fig. 14. LER(θ,φ) and ΔLER(θ,φ) for the indicated latitude $\times$ longitude boxes showing the decrease in LER over land and the increase over a small region Chile and Peru.

ACPD
12, 31991–32038, 2012

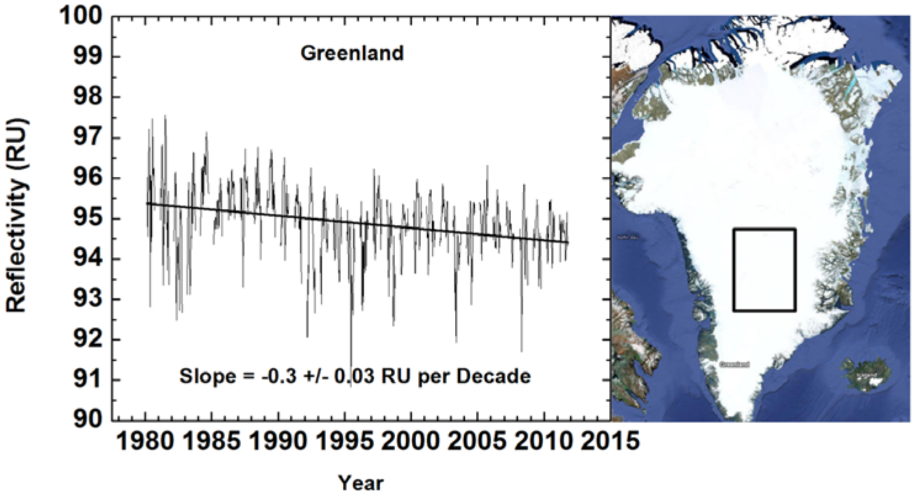

Fig. 15. LER(θ,φ) and ΔLER(θ,φ) for the indicated latitude × longitude box (71° N to 75° N and 37.5° W to 42.5° W) showing the decrease in LER over a portion of the Greenland ice cap away from coastal regions.

ACPD
12, 31991–32038, 2012

A net decrease in the Earth's cloud plus aerosol reflectivity 1979–2011

J. R. Herman et al.

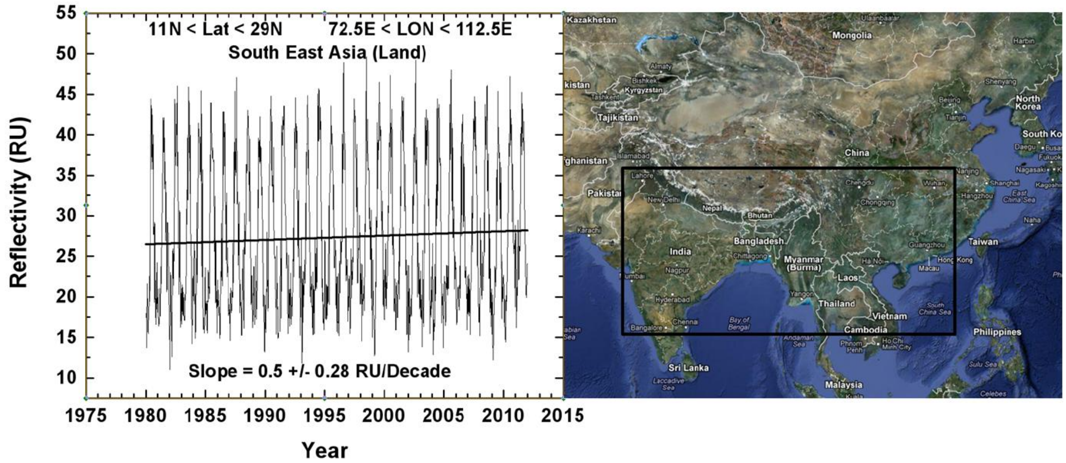

Fig. 16. LER(θ,φ) and ΔLER(θ,φ) for the indicated latitude × longitude box showing the increase in LER over India, Southern China, and Indochina.

ACPD
12, 31991–32038, 2012

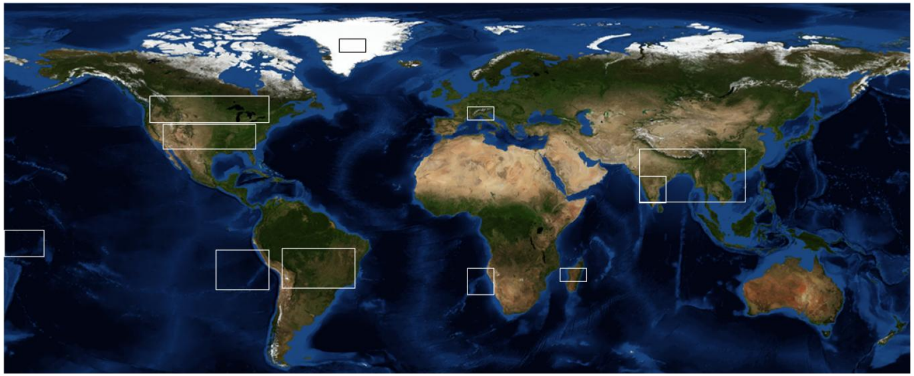

Fig. 17. Rectangular boxes represent interesting locations of selected sites for estimating LER trends based on the latitude × longitude trend maps shown in Fig. 11. The map is based on the Joint Polar Satellite System (JPSS) Visible Infrared Imaging Radiometer Suite (VIIRS).

ACPD
12, 31991–32038, 2012

A net decrease in the Earth's cloud plus aerosol reflectivity 1979–2011

J. R. Herman et al.